

Asymmetric Exclusion Process in a System of Interacting Brownian Particles

José Eduardo de Oliveira Rodrigues^{*} and Ronald Dickman[†]

*Departamento de Física, ICEx, Universidade Federal de Minas Gerais,
Caixa Postal 702, Belo Horizonte 30161-970, Minas Gerais, Brazil*

Abstract

We study a continuous-space version of the totally asymmetric simple exclusion process (TASEP), consisting of interacting Brownian particles subject to a driving force in a periodic external potential. Particles are inserted at the leftmost site at rate α , hop to the right at unit rate, and are removed at the rightmost site at rate β . Our study is motivated by recent experiments on colloidal particles in optical tweezer arrays. The external potential is of the form generated by such an array. Particles spend most of the time near potential minima, approximating the situation in the lattice gas; a short-range repulsive interaction prevents two particles from occupying the same potential well. A constant driving force, representing Stokes drag on particles suspended in a moving fluid, leads to biased motion. Our results for the density profile and current, obtained via numerical integration of the Langevin equation and dynamic Monte Carlo simulations, indicate that the continuous-space model exhibits phase transitions analogous to those observed in the lattice model. The correspondence is not exact, however, due to the lack of particle-hole symmetry in our model.

PACS numbers: 02.50.Ey, 05.60.Cd, 05.70.Fh

^{*}E-mail: jeo@fisica.ufmg.br

[†]E-mail: dickman@fisica.ufmg.br

I. INTRODUCTION

A driven lattice gas, or driven diffusive system, is a system of interacting particles that jump in a preferred direction on a lattice. The system cannot reach equilibrium but may attain a stationary state with a steady current; the model is a prototype for studies of nonequilibrium states [1–4]. The simplest example of a driven diffusive system, which has become one of the standard models of nonequilibrium statistical mechanics, is the totally asymmetric simple exclusion process (TASEP) [5–8]. In the TASEP with open boundaries the edge sites are connected to particle reservoirs with fixed densities. Introduced as a model of biopolymerization [9] and transport across membranes [10], over the years, this model has been applied to other processes, e.g., traffic flow [11], and cellular transport [12, 13].

From a mathematical point of view the model is of interest in the theory of interacting particle systems since, despite its simplicity, it shows a nontrivial behavior [7, 8, 14, 15]. In the one-dimensional TASEP with open boundaries, particles jump only to the right, along a one-dimensional lattice whose sites can be empty or occupied by a single particle. Particles are injected at the leftmost site at rate α if this site is empty, and removed at the rightmost site at rate β if this site is occupied. The one-dimensional TASEP, which has been solved exactly, exhibits three distinct phases in the α - β plane [16–19]. The phase transition is discontinuous along the line $\alpha = \beta < 1/2$, where the density profile is linear, and continuous along the lines $\alpha = 1/2$, $\alpha > \beta$ and $\beta = 1/2$, $\alpha < \beta$ (see Fig. 9). Although this model and variants have been the subject of intensive theoretical study, there is as yet no realization of a TASEP-like system in the laboratory.

The invention of optical tweezer arrays has permitted investigation of the dynamics of colloidal particles in an external periodic potential [20–25]. The motion at long times and low friction consists of jumps between adjacent potential min-

ima. If the particle and potential well sizes are chosen properly, only one particle can occupy a given well. The exclusion process is a caricature of this dynamics, suggesting that a system of colloidal particles in an optical tweezer array could be designed as a laboratory realization of the TASEP. Motivated by this possibility, we propose a model in continuous space having the same essential characteristics as the lattice TASEP. Our model represents colloidal particles immersed in a fluid flowing at constant rate through a one-dimensional optical tweezer array, restricting particle motion to the array axis. Specifically, we study a one-dimensional system of interacting Brownian particles subject to a periodic external potential, and to a constant external force representing the drag due to the fluid motion. A short-range (essentially hard-sphere) repulsion between particles prevents more than one particle occupying the same potential well. This continuous-space model is studied via numerical integration of Langevin equation and dynamic Monte Carlo simulation. We observe phase transitions similar to those found in the lattice TASEP. Some differences in the detailed behavior nevertheless appear, due to the lack of particle-hole symmetry in the continuous-space model. Details on the model and simulation methods are given in Sec. II and III. Simulation results are presented in Sec. IV, while our conclusions and prospects for future work are outlined in Sec. V.

II. CONTINUOUS-SPACE MODEL

Our aim is to study a continuous-space model sharing the same essential features as the TASEP (defined on a lattice), as a first step toward experimental realization of a TASEP-like system. The model should possess the following characteristics: i) confinement of particles to a one-dimensional structure; ii) localization of particles at potential minima (“wells”) of a linear periodic array with iii) multiple occupancy prohibited; iv) biased hopping between adjacent wells; v) insertion (removal) of par-

ticles at the initial (final) well. Criteria i)-iii) are realizable with a suitably tailored optical tweezer array. The array consists of a series of spherically symmetric optical tweezers; the particles flow along this line, which we take as the x axis. To avoid particles escaping the array, there should be a substantial overlap between neighboring wells, so that a potential maximum at a point midway between two wells is in fact a saddle point in the full three-dimensional space (see Fig. 1(a)). For a TASEP-like system, it is crucial that the probability of a particle escape from the array be negligible on the time-scale of the experiment. Effective confinement requires a potential barrier to escape the array much larger than $k_B T$; the barrier between adjacent minima should be smaller, to allow transitions between neighboring wells. In what follows we shall assume this condition is satisfied, and consider, for simplicity, a one-dimensional system. Fluctuations of the particle positions in the directions perpendicular to the array will therefore be ignored, but should be included in a more complete analysis.

The diameter of the optical tweezer well should be slightly greater than the particle diameter, so that at most one particle can occupy the well at a given time. Due to thermal fluctuations, particles can occasionally overcome the potential barrier separating neighboring wells. Since hopping must be asymmetric, we impose a steady fluid motion along the $+x$ axis, which effectively prohibits particle jumps in the opposite direction. In the lattice TASEP particles are inserted in the first site and removed from the last. Experimental realization of this feature is subtler, but can in principle be achieved with the help of optical tweezers at the beginning and end of the array, which drag particles into the first well and out of the last one at prescribed rates. We discuss an alternative method of insertion and removal in Sec. V.

The above sketch of an experimental setup motivates our study of Brownian motion of interacting colloidal particles in an optical tweezer array. The Langevin

equation for the i -th particle is

$$m\ddot{x}_i(t) = -b[\dot{x}_i(t) - v] - \frac{\partial V_{ext}(x_i)}{\partial x_i} - \frac{\partial}{\partial x_i} [V_{int}(x_{i,i-1}) + V_{int}(x_{i,i+1})] + m\Gamma_i(t), \quad (1)$$

where x_i , \dot{x}_i and \ddot{x}_i are, respectively, the position, velocity and acceleration of particle i , $x_{i,j} \equiv x_j - x_i$, and v is the terminal velocity of a particle in the moving fluid, in the absence of the periodic external potential V_{ext} . V_{int} is the (strongly repulsive) potential between neighboring particles. (We assume that the range of V_{int} to be short enough that only neighboring particles interact.) The first term on the right side of Eq. (1) represents damping of the particle velocity relative to the fluid. For a sphere of radius R , Stokes' Law gives:

$$b = 6\pi\mu R, \quad (2)$$

where μ is the fluid viscosity. Here it is important to stress that the fluid is three dimensional although we treat the particle motion as one dimensional. The final term is a random noise with the following properties:

$$\langle \Gamma_i \rangle = 0, \quad (3)$$

$$\langle \Gamma_i(t)\Gamma_j(t') \rangle = \frac{2bk_BT}{m^2}\delta_{i,j}\delta(t-t'), \quad (4)$$

where $k_B = 1.3806504 \times 10^{-23} J/K$ is Boltzmann's constant, T is temperature, and m is the particle mass. It is convenient to ignore the inertial term $m\ddot{x}_i(t)$ in Eq. (1), since the observational times of interest (microseconds or greater) are much larger than the relaxation time of the velocity, $m/b \sim 10^{-8} s$, for our choice of parameters. Then the velocity of particle i follows,

$$\dot{x}_i(t) = v - \frac{1}{b} \frac{\partial V_{ext}(x_i)}{\partial x_i} - \frac{1}{b} \frac{\partial}{\partial x_i} [V_{int}(x_{i,i-1}) + V_{int}(x_{i,i+1})] + \frac{m}{b} \Gamma_i(t). \quad (5)$$

A. Potentials

The potential of an optical tweezer array can be represented by a sum of n identical Gaussian profiles of width σ and spatial period d :

$$V_t(x) = -V_0 \sum_{n=0}^N e^{-(x-dn)^2/2\sigma^2}. \quad (6)$$

We require neighboring wells to overlap, which can be accomplished by setting $\sigma \lesssim d$; Figure 1(a) shows that this condition is satisfied for $\sigma = d/4$. For this choice of parameters, the potential is well approximated by a cosine, as can be seen from the Fourier coefficients

$$a_n = \frac{2}{d} \int_0^d \cos\left(\frac{2n\pi x}{d}\right) \left[- \sum_{n=0}^N e^{-(x-dn)^2/2\sigma^2} \right] dx. \quad (7)$$

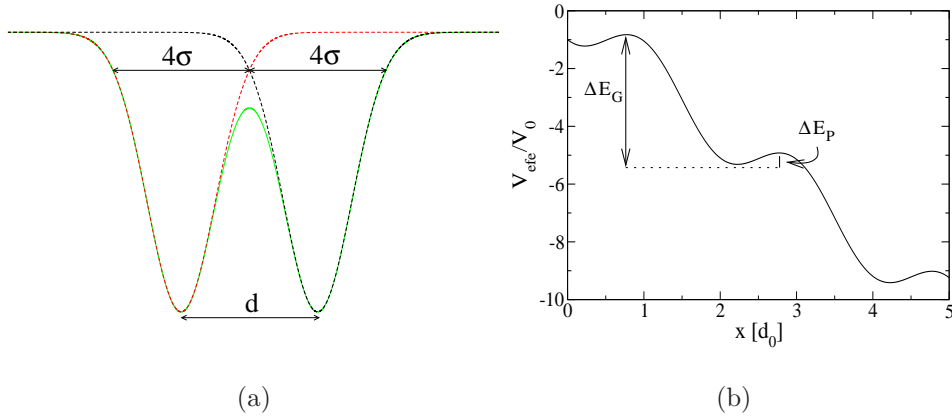


FIG. 1: (a) Two neighboring Gaussian profiles (red and black curves) and their sum (green); (b) effective external potential.

Numerical evaluation yields

$$\begin{aligned}
a_0 &= -0.627 \\
a_1 &= 0.365 \\
a_2 &= 9.010 \times 10^{-3}.
\end{aligned} \tag{8}$$

Note that $a_2/a_1 \simeq 0.025$, allowing us to write, to a good approximation, the array potential as a constant plus a cosine term. For the one-dimensional model studied here, we define

$$V_{ext}(x) = -V_0 \cos\left(\pi \frac{x}{d_0}\right) \tag{9}$$

as the periodic external potential.

The interaction between colloidal particles is taken as purely repulsive; for convenience we use a truncated $1/r^{12}$ potential:

$$V_{int}(r) = \begin{cases} U_0 \left[\left(\frac{a}{r}\right)^{12} - 1 \right], & r \leq a \\ 0, & r \geq a, \end{cases} \tag{10}$$

where a is the particle diameter and r distance between neighboring particles.

B. Parameter Values

To specify the external and interaction potentials, we need to fix V_0 and U_0 . These values must be chosen so as to approximate the TASEP dynamics given the length, time and energy scales characterizing the system. We measure lengths in units of microns, time in seconds and energies in units of $k_B T = 4.1419512 \times 10^{-21}$ J, assuming a temperature of 300K. We set $d_0 = 1$ (so that the period of the external potential is 2 microns), and take the particle diameter as $a = 1.8$, so that a pair of particles occupying neighboring wells have some freedom to fluctuate about the potential minimum. Taking the fluid as water (with viscosity $\mu = 0.01$ g/cm·s) we fix the friction coefficient as $b \cong 4.096 \text{ } k_B T \cdot \text{s}/(\mu\text{m})^2$.

To determine the fluid velocity v and external-potential intensity V_0 we examine the effective external potential, defined as

$$V_{eff} = -V_0 \cos\left(\pi \frac{x}{d_0}\right) - bvx, \quad (11)$$

i.e., the sum of external periodic potential and a fictitious potential representing the constant friction force acting on particles (see Fig. 1(b)). If $bvd_0 \gg V_0$, particles do not feel the periodic potential, while if $bvd_0 \ll V_0$ particle hopping is essentially unbiased. Let ΔE_G (ΔE_P) denote the difference between a given maximum of V_{eff} and the first minimum to the right (left) of this maximum. In this way, ΔE_G (ΔE_P) is the potential barrier separating a given potential minimum from its left (right) neighbor. A simple calculation shows that

$$\begin{aligned} \Delta E_G - \Delta E_P &= 2bvd_0, \\ \Delta E_G + \Delta E_P &= 4V_0 \cos(\pi x_0/d_0) + 4bvx_0, \end{aligned} \quad (12)$$

with

$$x_0 = \frac{d_0}{\pi} \sin^{-1}\left(\frac{bvd_0}{\pi V_0}\right), \quad (13)$$

such that the potential minima occur at $x_j = 2jd_0 + x_0$, and maxima at $y_j = 2jd_0 + 1 - x_0$ for j an integer. Given ΔE_G and ΔE_P , we can determine x_0 , v and V_0 . We take $\Delta E_P \sim k_B T$, and $\Delta E_G \gg k_B T$, so that a particle has a finite rate of jumping to the well on the right, and virtually no chance of jumping in the opposite direction. A good correspondence with lattice TASEP is obtained using $\Delta E_G = 20k_B T$ and $\Delta E_P = 2k_B T$. For these values we have,

$$\begin{aligned} v &= 2.1974 \mu\text{m/s} \\ V_0 &= 4.5680 k_B T \\ x_0 &= 0.2158 \mu\text{m}. \end{aligned} \quad (14)$$

To maintain the interparticle repulsion in the presence of the external potential, we must take U_0 substantially greater than V_0 . On the other hand, very large values

of U_0 are inconvenient for numerical integration of the Langevin equation, as a very small time increment would be required to avoid spurious particle displacements. We therefore use $U_0 = 40k_B T \simeq 9V_0$.

C. Single-particle dynamics

To begin, we consider a single Brownian particle moving in the system. Figure 2 shows a typical evolution of the particle position over time. The graph exhibits plateaux whose size corresponds to the time a particle stays in a given well. Studies of this kind allow us to determine the mean transition time τ between neighboring wells as $6.5380(9)\text{s}$. This quantity is needed in order to define the insertion and removal rates. (Recall that in the lattice TASEP these rates are defined in units of the hopping rate). If the first well is empty we insert a particle there (at the potential minimum position), at rate α/τ ; if the last well is occupied, we remove the particle at rate

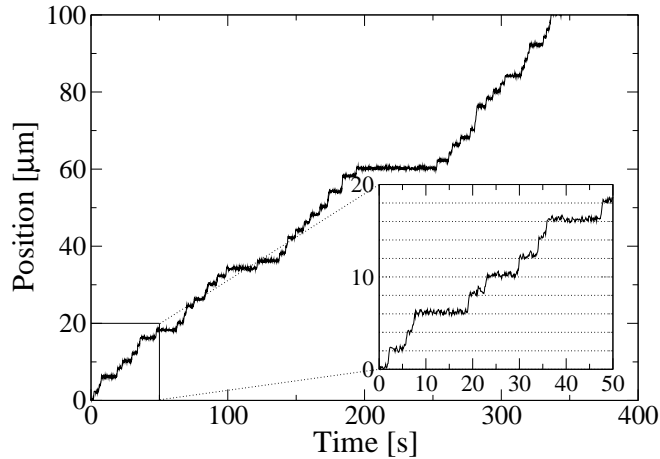


FIG. 2: Typical particle trajectory.

III. DYNAMIC MONTE CARLO SIMULATIONS

The Langevin simulation outlined in the preceding section is valuable for fixing the time scale of hopping between wells, and for confirming the basic phenomenology of the model. It is, however, rather inefficient numerically, so that it is desirable to implement a dynamic Monte Carlo (MC) simulation for large-scale studies. We apply the Metropolis algorithm to evolve the particle positions in time.

In this approach we use the following expression for the potential energy:

$$E = - \sum_{i=1}^N [V_0 \cos(\pi x_i) + bvx_i] + \sum_{i=1}^{N-1} V_{int}(x_{i+1} - x_i), \quad (15)$$

where V_{int} is given by Eq. (10). The drag force due to the moving fluid is represented by the effective potential $-bvx$. In the MC dynamics, a trial configuration is generated by selecting one of the N particles at random and subjecting it to a random displacement Δx , chosen from a Gaussian distribution with mean zero and standard deviation $\sigma = 0.2\mu\text{m}$. This value is 10% of the well size, large enough to afford a substantial speedup, but small enough that the probability of a particle displacement greater than $2\mu\text{m}$ is negligible. As is usual in Metropolis MC, trial moves such that the change in energy $\Delta E \leq 0$ are always accepted, while for $\Delta E > 0$ the trial move is accepted with probability $e^{-\Delta E/k_B T}$. We determine the mean number of Monte Carlo steps required for a particle move from one well to its neighbor on the right as $N_{MC} = 120.917(1)$. Thus the time per Monte Carlo step is

$$\tau_0 = \frac{\tau}{N_{MC}} = 5.4070(8) \times 10^{-2}\text{s}. \quad (16)$$

Particle insertion and removal are done as in the Langevin simulations. We verify below that this method is equivalent to the latter approach; the MC algorithm is ~ 1000 faster than numerical integration of the Langevin equation, for $L=100$.

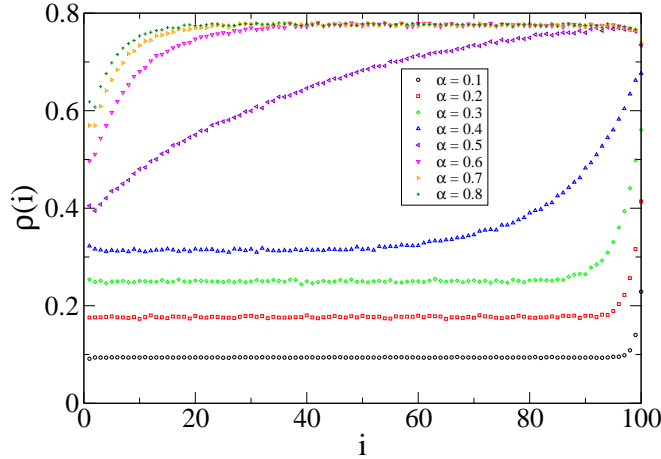


FIG. 3: Density profile for $\beta = 0.4$ obtained via numerical integration of the Langevin equation, for α values as indicated, $L = 100$.

IV. RESULTS

During the simulations we monitor the mean occupation probability $\rho(i)$ at each well i , and the current J , measured by the mean number of particles leaving the system per unit time. Examples of density profiles in the stationary regime ($\rho(i)$ versus i), are shown in Fig. 3 for several values of α , with $\beta = 0.4$. (From here on α and β are given in units of $1/\tau$, where τ is the mean time required for hopping between wells.) This figure shows that the continuous-space model exhibits the same basic phenomenology as the lattice TASEP. For $\alpha \leq 0.4$ the overall density grows with α . On increasing α from 0.4 to 0.5 there is a marked increase in density, but for further increases the density changes very little. While the Langevin simulation (LS) results already suggest that the model exhibits phase transitions, we shall use the more precise results of our MC simulations to perform a detailed analysis. Before proceeding, we verify that the MC method yields results in agreement with the LS. In Fig. 4 we compare density profiles obtained via LS and MC for the same values

of α and β . The bulk densities obtained using the two methods differ by $\leq 1.6\%$. Thus the MC method captures the behavior found using the Langevin equation to good precision.

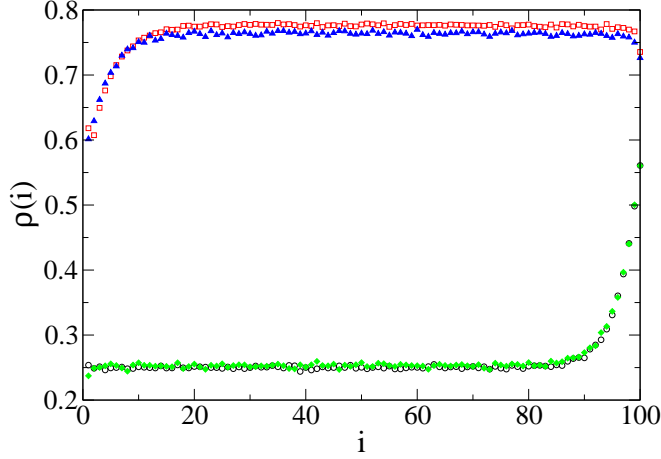


FIG. 4: Comparison between profiles obtained using LS (open symbols) and MC (filled symbols), $\alpha = 0.3$ (lower curves), $\alpha = 0.8$ (upper curves), $\beta = 0.4$, $L = 100$.

We perform MC simulations of systems of $L = 100, 200$ and 500 wells. Far from the phase transition, density profiles depend only weakly on system size, but near the transition there are significant finite-size effects, as illustrated in Fig. 5. In this case, as L increases, the profile tends to a near-constant value except for a sharp increase near the exit.

To minimize boundary effects we study the *bulk* density ρ , defined as the mean density over the 10% of sites nearest the center:

$$\rho = \frac{10}{L} \sum_{i=0.46L}^{0.55L} \rho(i). \quad (17)$$

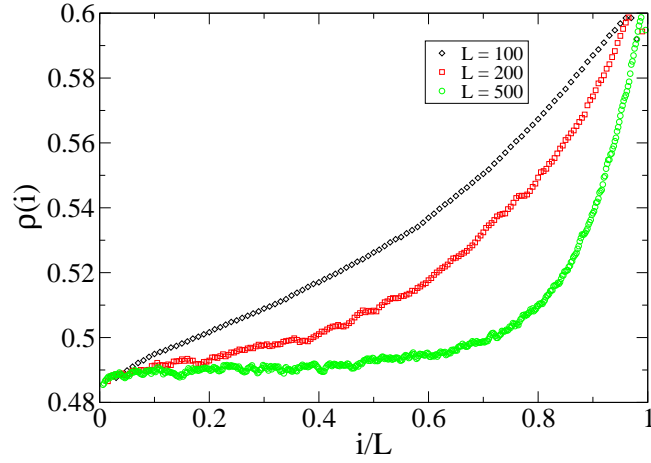


FIG. 5: Density ρ

and 500 wells.

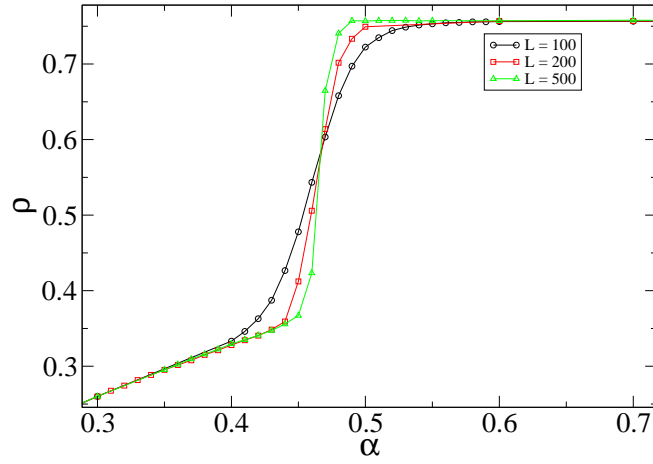


FIG. 6: Bulk density versus α for $\beta = 0.4$, system sizes $L = 100, 200$ and 500 .

The bulk density as a function of α , for $\beta = 0.4$, is shown in Fig. 6 for the three system sizes studied. These results strongly suggest the development of a discontinuity in $\rho(\alpha)$ near $\alpha = 0.47$ as the system size is increased.

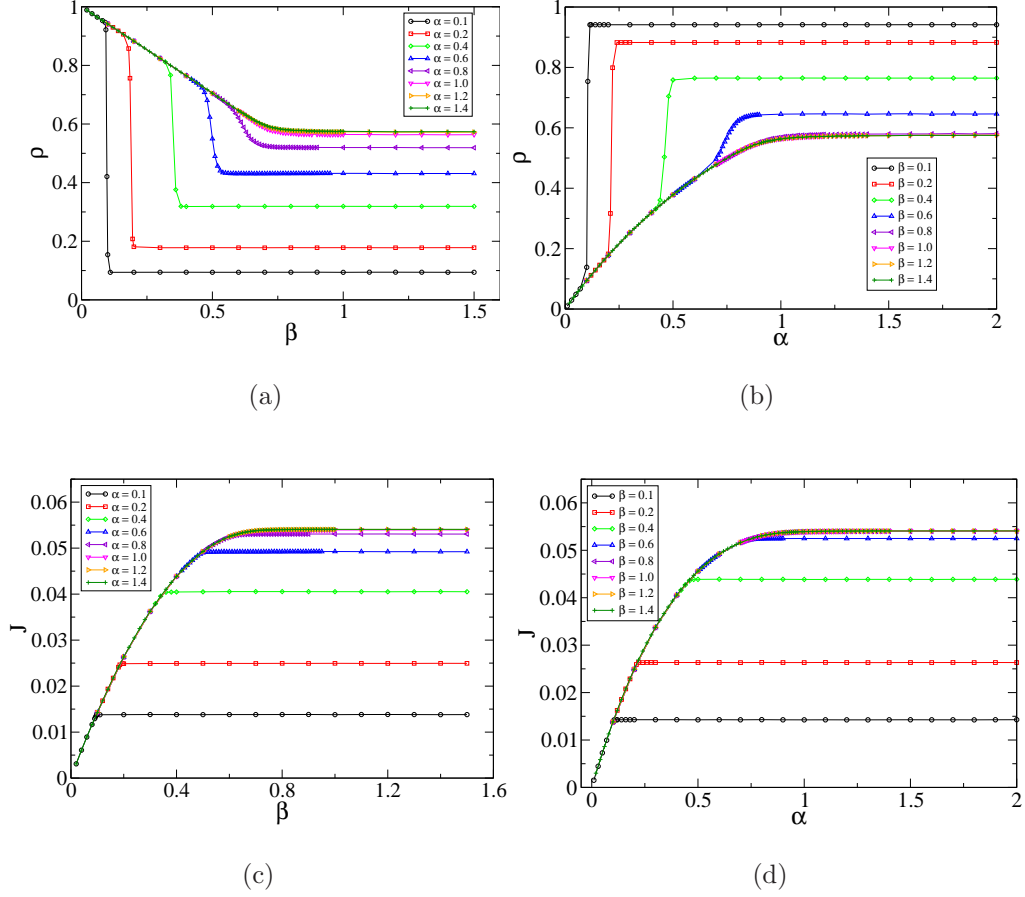


FIG. 7: Upper panels: bulk density for (a) fixed α and (b) fixed β . Lower panels: current for (c) fixed α and (d) fixed β . System size $L = 200$.

A. Phase diagram

Of principal interest in determining the phase diagram are the bulk density and the current as functions of the rates α and β . These results are summarized in Fig. 7, showing evidence of both continuous and discontinuous phase transitions, depending on the rates. We see that for low α ($\alpha < 0.8$ or so) and $\beta < \alpha$ the system is in the high-density phase, in which density and current depend only on β , whereas for $\beta > \alpha$, and $\beta < 0.6$ or so, the system is in the low-density phase in which density

and current depend only on α . For larger values ($\alpha > 0.8$ and $\beta > 0.6$), the system is in the maximum-current phase, in which density and current are independent of both α and β , and the current takes its maximum value. Thus the continuous-space model exhibits the same three phases observed in lattice model. As in the lattice model, the transition between the low- and high-density phases is discontinuous, whereas transitions between the maximum-current phase and the other phases are continuous. (While the density is discontinuous in the former case, the current is always continuous at the transition.)

We adopted the following procedure (“polynomial method”) to determine the values of (α, β) along the discontinuous transition line. Consider the case of fixed α . For small β , the stationary current depends only on β (see Fig. 7(c)). We therefore fit a polynomial $P(\beta)$ to the current in this regime, using data for a large, fixed α (in practice, $\alpha \geq 1.4$). For larger values of β , the current depends only on α ; in Fig. 7(c) this regime corresponds to one of the plateaux, $J = J^*(\alpha)$. The transition point $\beta_c(\alpha)$ is taken as the value at which the plateau intersects the polynomial fit to the small- β data, i.e., $P(\beta_c) = J^*(\alpha)$. Determination of $\alpha_c(\beta)$ follows an analogous procedure, in which we fit a polynomial to the current data for small α . We find that a quadratic polynomial is sufficient to fit (to within uncertainty) the current $j(\beta)$ at fixed α , while a good fit of $j(\alpha)$ (at fixed β) requires a quartic polynomial. In both cases the constant term in the polynomial is zero, since the current vanishes for α and/or β zero.

The above method is quite effective in locating points along the discontinuous transition line. Although it can in principle be used to locate continuous transitions as well, we found that in this case the estimates for α_c and β_c are rather sensitive to one’s choice of the range of values fit using the polynomial. We found the following approach (“derivative method”) to be more useful for continuous transition points. For fixed α , we estimate the derivative $dJ/d\beta$ using a spline fit (see Fig. 8). The

derivative decreases in a linear fashion with increasing β , except for a small roundoff region that we interpret as a finite-size effect. We then estimate β_c as the point where $dJ/d\beta$ falls to zero, using the data in the linear region. The procedure for fixed β is analogous. The continuous transition points obtained by this procedure are quite robust with respect to changes in the region analyzed, as long as we exclude the roundoff region.

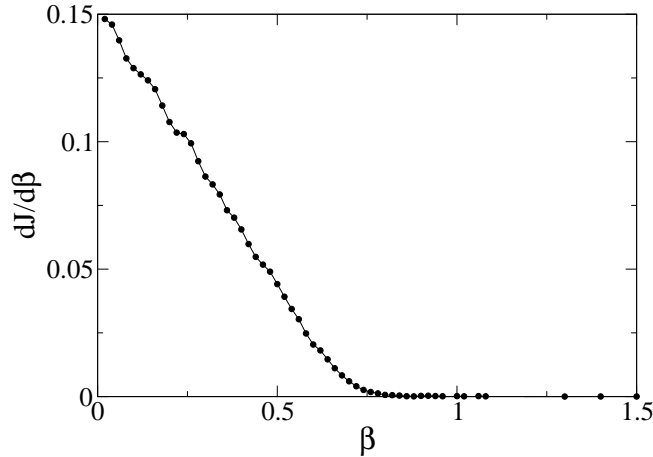


FIG. 8: Current derivative for $\alpha = 2.0$ and $L = 200$.

Using the methods described above we construct a phase diagram based on the data for each system size studied; that for $L = 500$ is shown in Fig. 9. The vertical boundary at $\alpha = 0.905(2)$, and the horizontal boundary at $\beta = 0.714(1)$ are obtained using the derivative method. (The polynomial method yields $\alpha = 0.8(1)$ and $\beta = 0.67(5)$, respectively, for these boundaries.) The grey triangle in Fig. 9 represents a region on which we could not determine precisely the phase boundaries using either method, due to numerical uncertainty and finite-size effects. While the simplest interpretation is that the three phase boundaries meet at the point of intersection between the continuous transitions (i.e., horizontal and vertical) lines, the data in

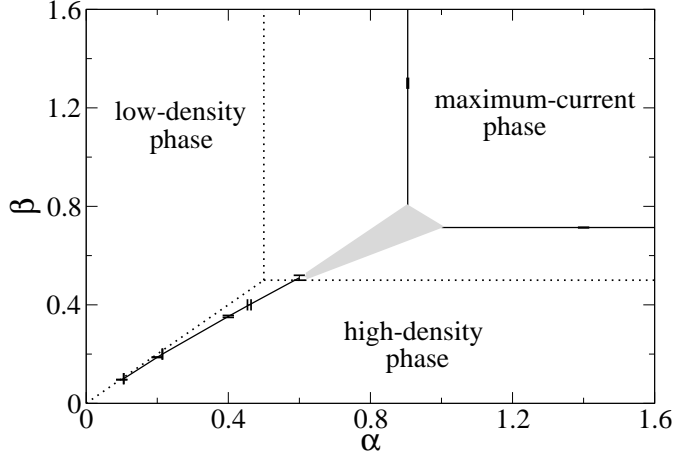


FIG. 9: Phase diagram of the TASEP on the lattice (dotted lines) and in continuous-space (solid lines) for $L=500$. The grey triangle denotes a region in which we are unable to determine the phase boundaries precisely.

hand are not sufficient to verify this.

The phase boundaries for $L = 100$ and $L = 200$ are nearly the same as for $L = 500$, suggesting that the latter are already quite close to limiting (infinite- L) values. Table I gives the α and β values for the continuous transition lines for the three sizes. There is little sign of systematic variation with system size, other than a small ($\sim 2.5\%$) increase in β_c on going from $L = 200$ to $L = 500$.

While the continuous-space phase diagram is isomorphic to that of the lattice model, there are some differences between the two cases that appear likely to persist in the infinite-size limit. Since the lattice model possesses particle-hole symmetry, the phase diagram is invariant under the exchange of α and β . Thus the boundary between the high- and low-density phases is a straight line extending from the origin to the point $(1/2, 1/2)$ in the α - β plane. The phase diagram of the continuous-space model does not possess this symmetry; the phase boundary between the high- and

L	α_c	β_c
100	0.901(4)	0.701(2)
200	0.901(2)	0.697(1)
500	0.905(2)	0.714(1)

TABLE I: Values of α and β at the continuous transitions obtained via the derivative method.

low-density phases does not fall along the line $\alpha = \beta$, and appears to be somewhat curved.

One might inquire whether the differences in the phase boundaries of the lattice and continuous-space models merely reflect finite-size effects in the latter. We have verified that in the *lattice* TASEP with $L = 200$, the phase boundaries fall quite near their expected (infinite-size) positions. Comparison of the phase boundaries (in continuous space) for $L = 200$ and 500 suggests that finite-size effects are somewhat stronger in the continuous space model than on the lattice. Given the lack of particle-hole symmetry, however, it appears very unlikely that the continuous-space phase boundaries will converge to those of the lattice model in the infinite-size limit.

The differences between the lattice and continuous-space models reflect, in part, the absence of particle-hole symmetry in the latter; particle positions fluctuate in continuous space, but are fixed in the lattice model. In continuous-space, moreover, particles occupying neighboring wells may influence one another via the repulsive potential V_{int} . On the lattice model no such influence exists, beyond simple exclusion. In continuous space, repulsive interactions should tend to spread particles more uniformly than on the lattice, promoting particle removal, and hindering insertion. Thus the transition from high to low density occurs for $\beta < \alpha$. Since repulsion is more significant for higher densities (i.e., larger α) the phase boundary should curve

toward the α axis, as is observed. The smaller value of β at the continuous transition (approximately 0.714(1) for $L = 500$), compared to that of α (about 0.905(2) for $L = 500$) may also be attributed to repulsion between neighboring particles.

B. Current: comparison with mean-field theory

The absence of particle-hole symmetry is again evident in a plot of the current as a function of density. In the lattice model, mean field theory gives $J = \rho(1 - \rho)$ [26, 27] which is in fact an exact expression. Fig. 10 compares the current on lattice with our results for continuous space. (Note that the latter exhibit virtually no finite-size effects on the scale of the figure.) Unlike in the lattice TASEP, here the current is not symmetric about $\rho = 1/2$; it takes its maximum value at a density of about 0.57. The fact that the maximum current occurs at a higher density than on the lattice may again be attributed to interparticle repulsion.

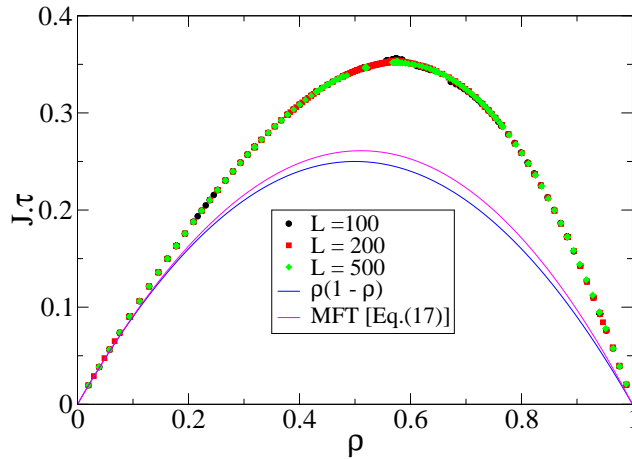


FIG. 10: Current *versus* density in the lattice model (exact) and the continuous-space model.

On the lattice, the current is equal to the probability of having an occupied site with its neighbor on the right vacant, i. e., $J = \langle \xi_i(1 - \xi_{i+1}) \rangle$, $\forall i$, where ξ_i is an indicator variable equal to one if site i is occupied and 0 if it is empty. In mean-field theory the joint probability is factored so: $\langle \xi_i(1 - \xi_{i+1}) \rangle = \langle \xi_i \rangle \langle (1 - \xi_{i+1}) \rangle$, and setting $\langle \xi_i \rangle = \rho$ in the bulk, we obtain $J = \rho(1 - \rho)$.

In developing a mean-field theory for the continuous-space model, one might argue that $J \simeq \rho(1 - \rho)/\tau$, i. e., that the current is simply given by the transition rate $1/\tau$ for jumps between neighboring wells times the probability of a given well being occupied and its right neighbor empty. Due to repulsive interactions between neighboring particles, however, a particle in the well to the left can also influence the hopping rate. As a first approximation we write

$$J = P(0, 1, 0)j(0, 1, 0) + P(1, 1, 0)j(1, 1, 0), \quad (18)$$

where $P(\xi_{i-1}, \xi_i, \xi_{i+1})$ is the joint probability for three adjacent wells, and $j(\xi_{i-1}, \xi_i, \xi_{i+1})$ is the transition rate in this configuration. Factorizing the joint probability, we have $P(0, 1, 0) = \rho(1 - \rho)^2$ and $P(1, 1, 0) = \rho^2(1 - \rho)$. It remains to evaluate the currents $j(0, 1, 0)$ and $j(1, 1, 0)$.

Consider first $j(0, 1, 0)$, the rate to overcome the barrier between wells i and $i + 1$, given that both $i - 1$ and $i + 1$ are empty. The mean first-passage time τ_{ca} , for a particle to overcome the barrier, is readily found via analysis of the one-dimensional Fokker-Planck equation. From the standard result [28] we have

$$\tau_{ca} = \frac{1}{k_B T} \int_a^c e^{U(x')/k_B T} dx' \int_{-\infty}^{x'} e^{-U(x'')/k_B T} dx'', \quad (19)$$

where $a = x_0$ and $c = x_0 + 2d_0$ are the positions of adjacent potential minima, with x_0 given by Eq. (13). Using the effective external potential, Eq. (11), for $U(x)$ (since there are no interactions with other particles), numerical evaluation of Eq. (19) yields $\tau_{ca} = 6.538 \text{ s} = 1/j(0, 1, 0)$. This value agrees to within uncertainty

with our simulation result for the mean time τ for a particle to hop between adjacent wells when there are no other particles in the system. Thus the mean-field curve in Fig. 10 agrees with simulation in the low-density limit.

To estimate the transition rate $j(1, 1, 0)$, we perform a Monte Carlo simulation to determine the mean time required for a particle to hop to the next well, when the preceding well is occupied, and there are no other particles in the system. This yields $1/j(1, 1, 0) = 5.548$ s. Although the presence of the trailing particle leads to an increase of about 18% in j , the effect is not sufficient to yield quantitative agreement with the current observed at higher densities (Fig. 10). There are two possible sources for this discrepancy. First, at moderate and high densities, strings of $n \geq 3$ occupied wells occur with finite probability, and the cumulative effect of repulsions along the chain should make the hopping rate of the lead particle an increasing function of n . Simulations of $n = 3 - 9$ occupied wells show that the transition rate of the first particle grows with n , but not enough to account for the maximum value of the current observed.

A second point is that the mean-field factorizations $P(0, 1, 0) = \rho(1 - \rho)^2$ and $P(1, 1, 0) = \rho^2(1 - \rho)$, are not very accurate in the continuous-space model. For density $\rho \simeq 0.52$, for example, we find

$$\frac{P(0, 1, 0)}{\rho(1 - \rho)^2} \simeq 1.21 \quad (20)$$

and

$$\frac{P(0, 1, 1)}{\rho^2(1 - \rho)} \simeq 1.04 \quad (21)$$

implying a significant correction to the mean-field theory predictions.

C. Fluctuations

To close this section we note an interesting finding on fluctuations. The variance of the density, as a function of α , with fixed β , exhibits a maximum at the discontinuous transition (see Fig. 11). For β values such that the transition is continuous, by contrast, no peak in $\text{var}(\rho)$ is observed at the transition. (Similar behavior is found, varying β with α fixed.) The large density fluctuations are associated with the presence of a shock separating high- and low-density regions, whose position fluctuates over the entire system. The position of maximum variance agrees to within uncertainty with the lines of the (discontinuous) phase transitions reported in Fig. 9. Analysis of the variance, however, appears to furnish less precise results than the method described above. The total energy exhibits fluctuations similar to those observed in the density, but we do not find any signal in $\text{var}(J)$ associated with the phase transitions.

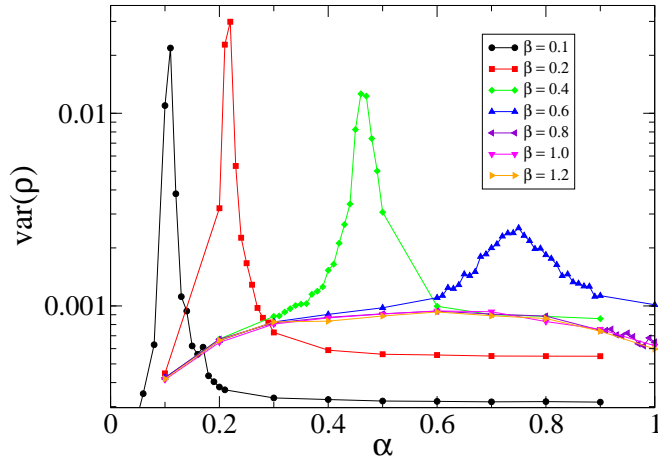


FIG. 11: Density variance versus α for β values as indicated. System size $L = 200$.

V. DISCUSSION

We propose a continuous-space model of interacting Brownian particles in a periodic potential as a possible realization of the TASEP. The particles are subject to a constant drive in a periodic external potential. Using numerical integration of the Langevin equation and Monte Carlo simulation, we study systems of $L = 100, 200$, and 500 wells. Our results show that the continuous-space model exhibits continuous and discontinuous phase transitions analogous to those observed in the lattice TASEP. The phase diagram of the continuous-space model is similar to that of the lattice model, but exhibits some differences due to the absence of particle-hole symmetry. This difference appears to be associated with fluctuations of particle positions around potential minima. Such fluctuations, together with the repulsive interactions between neighboring particles, cause the current to attain its maximum value at a density somewhat greater than $1/2$, the density marking the maximum current in the lattice model. We expect these changes (relative to the lattice model) to be generic for continuous-space systems exhibiting TASEP-like phase transitions.

We believe that the present study demonstrates the possibility of observing TASEP-like behavior in laboratory experiments on systems of interacting colloidal particles in a one-dimensional optical tweezer array. The essential features of the TASEP - localization of particles in potential wells, with multiple occupancy prohibited, and bias hopping along the line - are readily accomplished with a appropriate choice of particle, fluid, and tweezer array parameters. It is however less obvious how to implement random insertion and removal of particles at the first and last wells of the array. Particle manipulation can be accomplished using optical tweezers to transfer particles between wells and reservoirs. To transfer particles in a random fashion, these tweezers would have to be intrinsically noisy or chaotic, controlled by a random number generator, or driven by a noise signal. A simpler alternative may

be *periodic* insertion and removal. In this case, one inserts a particle into the first well (when empty) at intervals of τ/α , and checks for occupancy of the final well at intervals of τ/β , removing the particle if the well is occupied.

A preliminary study of the continuous-space model using periodic insertion and removal confirms that the three TASEP phases are again found. The density profiles under periodic and random particle transfer are very similar in the maximum current phase, where the density profile is insensitive to small changes in the insertion and removal rates. Small systematic differences do however appear in the other phases, as shown in Fig. 12.

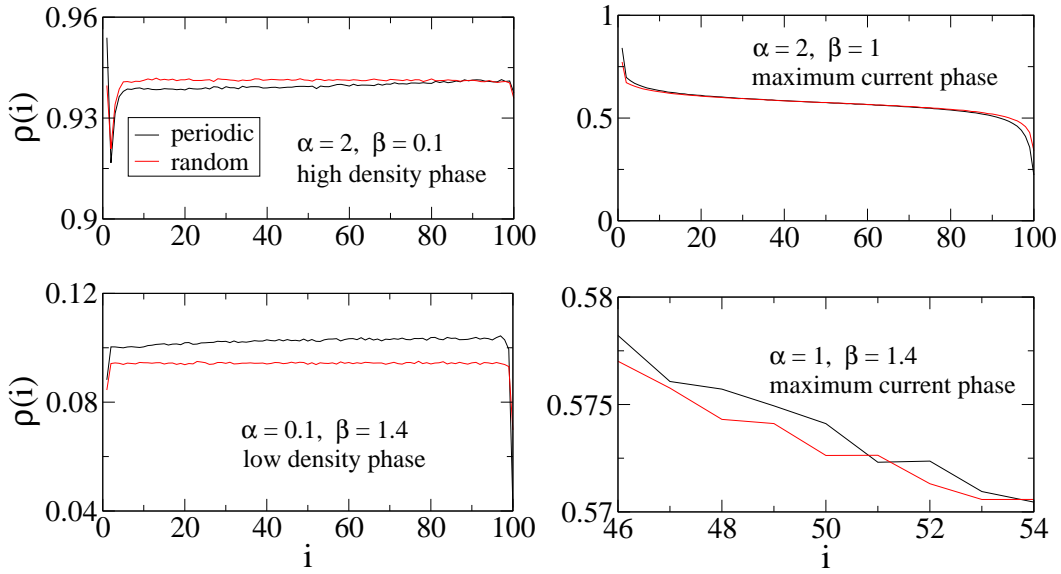


FIG. 12: Comparison of density profiles obtained using periodic (black) and random (red) insertion and removal, $L = 100$.

Although our study strongly suggests the feasibility of a laboratory realization of the TASEP, a number of additional features would have to be included in the model, before a quantitative comparison with experiment could be made. The principal

modifications we expect to be necessary are study of a three-dimensional model, allowing fluctuations in directions perpendicular to the array axis, and inclusion of hydrodynamic interactions between the particles. We defer these tasks to future work.

Acknowledgments

We thank O. N. Mesquita, U. Agero and J. G. Moreira for helpful comments. This work was supported by CNPq and Fapemig, Brazil.

-
- [1] B. Schmittmann and R. K. P. Zia, in *Phase Transitions and Critical Phenomena*, edited by C. Domb and J. L. Lebowitz (Academic Press, London, 1995), Vol. 17; Phys. Rep. **301**, 45 (1998).
 - [2] J. Marro and R. Dickman, *Nonequilibrium Phase Transition in Lattice Models* (Cambridge University Press, Cambridge, 1999).
 - [3] Katz, J. L. Lebowitz, and H. Spohn, Phys. Rev. B **28**, 1655 (1983).
 - [4] K.-t. Leung, B. Schmittmann, and R. K. P. Zia, Phys. Rev. Lett. **62**, 1772 (1989).
 - [5] J. T. MacDonald, J. H. Gibbs, and A. C. Pipkin, Biopolymers **6**, 1 (1968).
 - [6] E. D. Andjel, M. Bramson, and T. M. Liggett, Prob. Theory Rel. Fields **78**, 231 (1988).
 - [7] T. E. Harris, J. Appl. Probab. **2**, 323 (1965).
 - [8] F. Spitzer, Adv. Math. **5**, 2 (1970).
 - [9] J. T. MacDonald and J. H. Gibbs, Biopolymers **7**, 707 (1969).
 - [10] K. Heckmann, in *Passive Permeability of Cell Membranes*, edited by F. Kreuzer and J. F. G. Slegers (Plenum, New York, 1972), Vol. 3, p. 127.
 - [11] A. Schadschneider, Phys. A **285**, 101 (2001).

- [12] G. von Heijne, C. Blomberg, and H. Liljenström, *J. Theor. Biol.* **125**, 1 (1987).
- [13] V. Kukla, J. Kornatowski, D. Demuth, I. Girnus, H. Pfeifer, L. Rees, S. Schunk, K. Unger, and J. Kärger, *Science* **272**, 702 (1996).
- [14] T. M. Liggett, in *Interacting Particle Systems*, edited by D. G. Crane (Springer, New York, 1985); in *Stochastic Interacting systems: Contact, Voter and Exclusion Process*, edited by D.G. Crane (Springer, Berlin, 1999).
- [15] H. Spohn, *Large scale dynamics of interacting particles* (Springer, New York, 1991).
- [16] G. Schütz and E. Domany, *J. Stat. Phys.* **72**, 277 (1993).
- [17] B. Derrida, M. R. Evans, V. Hakim, and V. Pasquier, *J. Phys. A: Math. Gen.* **26**, 1493 (1993).
- [18] B. Derrida and M. R. Evans, *The asymmetric exclusion model: exact results through a matrix approach in nonequilibrium statistical mechanics in one dimension* (Cambridge University Press, Cambridge, 1996).
- [19] B. Derrida, *Phys. Rep.* **301**, 65 (1998).
- [20] J. M. Sancho, A. M. Lacasta, K. Lindenberg, I. M. Sokolov, and A. H. Romero, *Phys. Rev. Lett.* **92**, 250601 (2004).
- [21] P. T. Korda, M. B. Taylor, and D. G. Grier, *Phys. Rev. Lett.* **89**, 128301 (2002).
- [22] M. P. Macdonald, G. C. Spalding, and K. Dholakia, *Nature* **421**, 421 (2003).
- [23] P. Y. Chiou, A. T. Ohta, and M. C. Wu, *Nature (London)* **436**, 370 (2005).
- [24] A. M. Lacasta, J. M. Sancho, A. H. Romero, and K. Lindenberg, *Phys. Rev. Lett.* **94**, 160601 (2005).
- [25] Y. Roichman, V. Wong, and D. G. Grier, *Physical Review E* **75**, 011407 (2007).
- [26] J. Krug, *Phys. Rev. Lett.* **67**, 1882 (1991).
- [27] B. Derrida, E. Domany, and D. Mukamel, *J. Stat. Phys.* **69**, 667 (1992).
- [28] N. G. van Kampen, *Stochastic Processes in Physics and Chemistry* (Elsevier, Amsterdam, 2007).